

# REMOVAL EFFICIENCY AND MECHANISM OF REFRACTORY ORGANIC MATTER FROM LANDFILL LEACHATE MBR EFFLUENT BY THE MoS<sub>2</sub>-RNHANCEG Fe<sup>0</sup>/H<sub>2</sub>O<sub>2</sub> SYSTEM

Jing Yang<sup>1</sup>, Xiaoqin Zhang<sup>2</sup>, Jia Tang<sup>3</sup>, Jinlan Li<sup>4</sup>, Aiping Zhang<sup>\*</sup>  
College of Chemistry and Materials Science, Sichuan Normal University,  
Chengdu 610066, China

## ABSTRACT

In this study, molybdenum disulfide (MoS<sub>2</sub>) was used to enhance a zero-valent iron/hydrogen peroxide (Fe<sup>0</sup>/H<sub>2</sub>O<sub>2</sub>) Fenton-like system, which was able to remove refractory organic matter from the effluent produced during the treatment of landfill leachate by a membrane bioreactor (MBR). The MoS<sub>2</sub>/Fe<sup>0</sup>/H<sub>2</sub>O<sub>2</sub> system could efficiently remove refractory organic matter (i.e., fulvic acid-like substances and humic-like substances) from the MBR effluent and also exhibited a strong synergistic effect. Under the conditions of initial pH=3, H<sub>2</sub>O<sub>2</sub>=40 mmol/L, Fe<sup>0</sup>=0.4 g/L, MoS<sub>2</sub>=0.1 g/L, and t=30 min, compared with a Fe<sup>0</sup>/H<sub>2</sub>O<sub>2</sub> system, the absorbance UV<sub>254</sub>, chroma (CN), and total organic carbon (TOC) removal rates in MBR effluent treated with MoS<sub>2</sub>/Fe<sup>0</sup>/H<sub>2</sub>O<sub>2</sub> increased to 48.68%, 63.85%, and 35.85%, respectively. Through the identification of reactive oxygen species (ROS), the hydroxyl radical (HO<sup>•</sup>) concentration and an analysis of the effective utilization rate of H<sub>2</sub>O<sub>2</sub>, as well as an analysis of the morphology of the material, the distribution of Fe compounds, valence changes, and the Fe ion concentration, it was proven that MoS<sub>2</sub> promoted the cycling of Fe<sup>3+</sup>/Fe<sup>2+</sup> in the Fe<sup>0</sup>/H<sub>2</sub>O<sub>2</sub> process. The addition of MoS<sub>2</sub> promoted the Fe<sup>3+</sup>/Fe<sup>2+</sup> cycling reaction through the exposed Mo<sup>4+</sup> active center, significantly promoting the decomposition of H<sub>2</sub>O<sub>2</sub> and the formation of HO<sup>•</sup>. The MoS<sub>2</sub>/Fe<sup>0</sup>/H<sub>2</sub>O<sub>2</sub> system was able to remove a wide range of aromatic organics, indicating the wide applicability of the system. This study developed a new method for the efficient removal of refractory organic matter from landfill leachate.

## 1 INTRODUCTION

In recent years, with the rapid development of

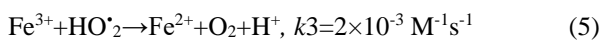
China's economy and the continuous improvement of living standards, the production of urban household waste has grown. According to the *China Statistical Yearbook*, the total output of urban domestic waste in 2020 was 235 million tons. To satisfy the growing need for waste disposal, the number of landfills and incineration plants has increased in recent years. However, a large amount of secondary effluent, i.e., landfill leachate, will inevitably be produced in the treatment of sanitary landfill or incineration effluent. Landfill leachate is a special wastewater that is extremely difficult to treat. It usually contains high concentrations of refractory organic matter, ammonia nitrogen, inorganic salts, and heavy metal ions. With the prolongation of landfill life and the stabilization of municipal solid waste (MSW), the molecular composition of organic matter in landfill leachate will become more complex, and its chemical structure will stabilize, inhibiting biodegradation. If landfill leachate is discharged without strict treatment, it will cause considerable pollution to the surrounding environment.

In practical applications, due to the low cost of biological treatment technologies, a biological treatment is usually applied to remove most of the organic matter in landfill leachate. However, further treatment methods are required to fully treat the biologically treated leachate and satisfy the strict discharge requirements. Currently, the most commonly used treatment methods include multistage membrane treatment, advanced oxidation processes (AOPs), and other combined systems.

The application of membrane treatment to landfill leachate can produce wastewater that satisfies discharge requirements, but this technology is controversial because of the other issues it raises (e.g., membrane contamination and production of leachate concentrate).

Advanced oxidation processes are chemical oxidation methods that use reactive oxygen species (ROS) with a high redox potential to degrade and even mineralize organic matter.

In recent years, zero-valent iron ( $\text{Fe}^0$ ) has attracted much attention as an environmentally sustainable and cost-effective material for the removal of various environmental pollutants, especially as a promising alternative source of the  $\text{Fe}^{2+}$  activator in heterogeneous Fenton reactions. Thus, a zero-valent iron-hydrogen peroxide combined system ( $\text{Fe}^0/\text{H}_2\text{O}_2$ ) has been developed as a Fenton-like system for treating organic wastewater. Under acidic conditions,  $\text{Fe}^{2+}$  can be gradually released from  $\text{Fe}^0$  (Eq. (1)) to activate  $\text{H}_2\text{O}_2$ . In addition,  $\text{Fe}^0$  can be oxidized by  $\text{H}_2\text{O}_2$  to produce  $\text{Fe}^{2+}$ ; thus, contributing to the degradation of organic matter. In addition, iron (hydrogen) oxides generated on the surface of  $\text{Fe}^0$  can also heterogeneously activate  $\text{H}_2\text{O}_2$ , further promoting the degradation of organic matter.

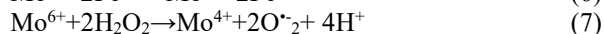


The rate-limiting step of Eq. (4) determines the overall efficiency of the reaction. Even under the action of the activator, the efficiency of this reaction is still very low, requiring excessive amounts of  $\text{H}_2\text{O}_2$  and activator, which makes the large-scale application of AOPs uneconomical in wastewater treatment. In addition, the activity of the  $\text{Fe}^0$  activator is affected by the formation of a passivation layer of iron oxide on the surface, and the  $\text{Fe}^{2+}/\text{Fe}^{3+}$  cycle reaction (Eq. (4) and (5)) is not fast enough, which greatly reduces the removal efficiency of  $\text{Fe}^0/\text{H}_2\text{O}_2$  systems for landfill leachate treatment. There is an urgent need to improve this system to overcome the inefficient conversion between  $\text{Fe}^{2+}$  and  $\text{Fe}^{3+}$  ions.

Promoting the  $\text{Fe}^{3+}/\text{Fe}^{2+}$  redox cycle has the potential for further developing AOPs, and studies of AOPs in this field have focused on the use of organic acids as Fe chelators to complex  $\text{Fe}^{3+}$  and provide electrons to promote the  $\text{Fe}^{3+}/\text{Fe}^{2+}$  redox cycle. However, the above methods can also cause secondary pollution and make it difficult to completely mineralize organic molecules.

It has been proven that metal sulfides (molybdenum

disulfide ( $\text{MoS}_2$ ), tungsten disulfide ( $\text{WS}_2$ , etc.) are excellent materials for improving the efficiency of  $\text{H}_2\text{O}_2$  decomposition and will significantly reduce the amount of  $\text{H}_2\text{O}_2$  and  $\text{Fe}^{2+}$  needed. According to previous studies, the surface of  $\text{MoS}_2$  contains unsaturated S atoms, and will capture protons to form  $\text{H}_2\text{S}$ ; thus, exposing the reductive metal active center  $\text{Mo}^{4+}$  to promote the rate-limiting reaction of the  $\text{Fe}^{3+}/\text{Fe}^{2+}$  redox cycle and the formation of  $\text{Mo}^{6+}$ . After the Fenton reaction,  $\text{Mo}^{6+}$  is further reduced to  $\text{Mo}^{4+}$  with the help of  $\text{H}_2\text{O}_2$ , ensuring the cycling of  $\text{MoS}_2$  (Eq. (6) and (7)).



Using an  $\text{Fe}^0/\text{H}_2\text{O}_2$  system, in this study  $\text{MoS}_2$  was applied as an additive to degrade the effluent produced during the treatment of landfill leachate by a membrane bioreactor (MBR). The aims of the study were: (1) to study the synergistic effect of the  $\text{MoS}_2/\text{Fe}^0/\text{H}_2\text{O}_2$  system for the removal of MBR effluent; (2) to study the effect of important factors controlling the degradation of MBR effluent; (3) to propose a possible degradation pathway of organic matter in the  $\text{MoS}_2/\text{Fe}^0/\text{H}_2\text{O}_2$  process and identify the mechanism by which  $\text{MoS}_2$  is enhanced in a heterogeneous Fenton reaction.

## 2 MATERIALS AND METHODS

### 2.1 The MBR effluent used in the experiment

The leachate samples used in this study were collected from the MBR effluent of a large anaerobic landfill located in southwest China. The landfill was built in 1992 and had been in operation for 28 years at the time of sampling. The leachate was yellow-brown with no obvious odor,  $\text{pH}=8.27$ , total organic carbon ( $\text{TOC}$ )= $189.70 \text{ mg/L}$ , absorbance ( $\text{UV}_{254}$ )= $5.69 \text{ cm}^{-1}$ , and chroma ( $\text{CN}$ )= $0.3577$ . After the leachate was collected in a 25 L blue polyethylene plastic bucket, it was immediately sealed and stored in a cool dry place in the laboratory away from light.

## 3. RESULTS AND DISCUSSION

### 3.1 The performance of the $\text{MoS}_2/\text{Fe}^0/\text{H}_2\text{O}_2$ system

To investigate the effectiveness of the  $\text{MoS}_2/\text{Fe}^0/\text{H}_2\text{O}_2$  system on refractory organic matter in MBR effluent, the removal effect, and the structure and humus content of refractory organic matter in MBR effluent treated by different systems ( $\text{Fe}^0$  alone,  $\text{H}_2\text{O}_2$

alone, MoS<sub>2</sub> alone, H<sub>2</sub>O<sub>2</sub>/MoS<sub>2</sub>, MoS<sub>2</sub>/Fe<sup>0</sup>, and Fe<sup>0</sup>/H<sub>2</sub>O<sub>2</sub>) were compared in controlled experiments.

### 3.1.1: Removal rate of refractory organic matter

As shown in Fig. 1(a), when pH=3 and the reaction time was 30 min, the leachate was hardly degraded under the conditions of Fe<sup>0</sup> alone, H<sub>2</sub>O<sub>2</sub> alone, and MoS<sub>2</sub> alone. The decolorization rates of the MBR effluent in the MoS<sub>2</sub> alone, H<sub>2</sub>O<sub>2</sub>/MoS<sub>2</sub>, and Fe<sup>0</sup>/MoS<sub>2</sub> systems were 30.60%, 21.04%, and 21.74%, respectively. This may be related to the adsorption of MoS<sub>2</sub>, mainly due to the van der Waals forces and electrostatic attraction between MoS<sub>2</sub> and organic matter. A relatively lower treatment efficiency of H<sub>2</sub>O<sub>2</sub>/MoS<sub>2</sub> was observed comparing to that of MoS<sub>2</sub>, it could be attributed to that MoS<sub>2</sub> cannot activate H<sub>2</sub>O<sub>2</sub> and instead MoS<sub>2</sub> could be oxidized by H<sub>2</sub>O<sub>2</sub>, affecting the adsorption effect of MoS<sub>2</sub> as well as the oxidation effect of H<sub>2</sub>O<sub>2</sub>. The UV<sub>254</sub>, CN, and TOC removal rates from the MBR effluent by Fe<sup>0</sup>/H<sub>2</sub>O<sub>2</sub> were 36.2%, 51.83%, and 27.94%, respectively. The heterogeneous Fenton reaction based on Fe<sup>0</sup>/H<sub>2</sub>O<sub>2</sub> (Eq. (2) and (3)) produced a large amount of HO<sup>•</sup>. Because HO<sup>•</sup> can react with biological macromolecules, as well as different types of organic and inorganic matter, and has a high reaction constant and negative charge electrophilicity, it attacks organic pollutant molecules by hydrogen extraction, electrophilic addition, and electron transfer. However, under conditions with the same oxidant and Fe<sup>0</sup>, the UV<sub>254</sub>, CN, and TOC removal rates in the MoS<sub>2</sub>/Fe<sup>0</sup>/H<sub>2</sub>O<sub>2</sub> system were 48.68%, 63.85%, and 35.85%, respectively, within 30 min, which were higher than in the other systems. In addition, compared with the Fe<sup>0</sup>/H<sub>2</sub>O<sub>2</sub> system, the reaction rate in the MoS<sub>2</sub>/Fe<sup>0</sup>/H<sub>2</sub>O<sub>2</sub> system increased from 1.30 to 2.02 min<sup>-1</sup> (Fig. 1(b)), indicating that the addition of a small amount of MoS<sub>2</sub> may accelerate the Fe<sup>3+</sup>/Fe<sup>2+</sup> redox cycle (Eq. (3) and (6)). Therefore, Fe<sup>2+</sup> activated H<sub>2</sub>O<sub>2</sub>, producing more HO<sup>•</sup> to react with organic pollutant molecules.

### 3.1.2: Changes in the structure of organic matter

The MBR effluent contained a large amount of organic matter with complex structures. The presence of these compounds was confirmed by the absorbance at 200–600 nm in the UV–vis spectrum of the leachate, as shown in Fig. S1. The leachate after treatment had no obvious absorption peak, indicating that it contained a large amount of dissolved organic matter.

The overall absorbance of the MBR effluent treated by the MoS<sub>2</sub>/Fe<sup>0</sup>/H<sub>2</sub>O<sub>2</sub> system was lower than that in the

other systems. This indicated that the MoS<sub>2</sub>/Fe<sup>0</sup>/H<sub>2</sub>O<sub>2</sub> system was effective for breaking down the complex structures of refractory organic matter. Specific absorbances at 254 and 280 nm (A<sub>254</sub> and A<sub>280</sub>, respectively) are commonly used to characterize the degree of aromatization of organic matter. The A<sub>300</sub>/A<sub>400</sub>, A<sub>240</sub>/A<sub>420</sub>, and A<sub>250</sub>/A<sub>365</sub> ratios are used to characterize the degree of polymerization, the structuralization of humic acid, and the molecular weight of organic matter, respectively. The higher the ratio, the lower the degree of polymerization, structuralization, and molecular weight of the organic matter. The absorbance at wavelengths of 226–400 nm was mainly caused by the structure of benzene rings in a variety of conjugated compounds, and the integration of absorbance in this range was used to analyze the variation in aromatic compounds. As shown in Table S1, the MoS<sub>2</sub>/Fe<sup>0</sup>/H<sub>2</sub>O<sub>2</sub> system effectively degraded aromatic organic matter containing benzene rings in the leachate, and the system also effectively reduced the molecular weight, as well as the degree of polymerization and structuralization of the organic matter.

### 3.1.3: Changes in the humus

The 3D-EEM spectra were used to analyze the changes in the humus in the leachate during the treatment by different systems. As shown in Fig. 1(c–j), there were two maximum fluorescence peaks in the 3D fluorescence of the MBR effluent. Peak A (Ex/Em = 250/460 nm, intensity=3625 au, humic acid-like fluorescence in the UV region) was mainly caused by low molecular weight organic matter with a high fluorescence frequency. Peak C (Ex/Em = 325/410 nm, intensity=2578 au, humic acid/fulvic acid-like fluorescence in the visible region) was mainly caused by relatively stable large molecular weight aromatic organic matter. Therefore, the leachate used in this study was difficult to degrade.

It can be clearly observed in Fig. 1(i) and (j) that the 3D-EEM fluorescence in the Fe<sup>0</sup>/H<sub>2</sub>O<sub>2</sub> and MoS<sub>2</sub>/Fe<sup>0</sup>/H<sub>2</sub>O<sub>2</sub> systems weakened after 30 min of reaction compared with the other systems. Table S2 shows that the intensities of peaks A and C in the MoS<sub>2</sub>/Fe<sup>0</sup>/H<sub>2</sub>O<sub>2</sub> system were weaker than those in the Fe<sup>0</sup>/H<sub>2</sub>O<sub>2</sub> system, with the lowest intensities reaching 1001.0 and 1091.0 au. The humus removal rate of this system in the UV and visible regions was 72.4% and 57.7%, respectively.

The peak A/peak C fluorescence peak intensity ratios for the H<sub>2</sub>O<sub>2</sub> alone, Fe alone, MoS<sub>2</sub> alone, Fe<sup>0</sup>/MoS<sub>2</sub>, and H<sub>2</sub>O<sub>2</sub>/MoS<sub>2</sub> systems did not differ much

from those of the MBR effluent raw water. The peak A/peak C ratios for the  $\text{Fe}^0/\text{H}_2\text{O}_2$  and  $\text{MoS}_2/\text{Fe}^0/\text{H}_2\text{O}_2$  systems were much lower than those of the MBR effluent raw water, and there was an obvious blueshift of peak A, indicating a degree of molecular condensation and molecular weight decomposition. Additionally, the organic matter content of the leachate was greatly reduced, which was due to the nonselective oxidation property of  $\text{HO}^\bullet$ . It also had a strong effect on organic matter with a low molecular weight and high fluorescence frequency. The  $\text{MoS}_2/\text{Fe}^0/\text{H}_2\text{O}_2$  system significantly improved the degradation of humus in leachate.

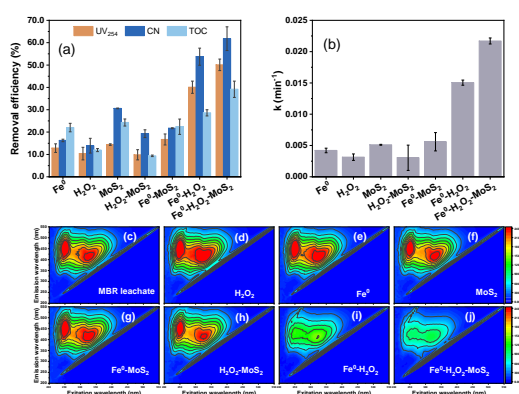


Fig 1 The influence of different treatment systems on organic matter removal efficiency (a) and reaction rate (b). (c-j) The 3D-EEM spectra of MBR effluent treated by different systems

### 3.1.4: Quantitative analysis of $\text{HO}^\bullet$ and effective utilization of $\text{H}_2\text{O}_2$

Tert-Butanol (TBA) is an efficient  $\text{HO}^\bullet$  scavenger with reaction rate constants ranging from  $3.8$  to  $7.7 \times 10^8 \text{ M}^{-1}\text{s}^{-1}$ . Because TBA affected the TOC concentration of the MBR effluent, but had no effect on the absorbance in the UV region,  $\text{UV}_{254}$  was used as the evaluation index of the refractory organic matter content of the MBR effluent. As shown in Fig. 2(a), after adding TBA to the  $\text{MoS}_2/\text{Fe}^0/\text{H}_2\text{O}_2$  system, the  $\text{UV}_{254}$  of the MBR effluent decreased to different degrees. When the mole ratio of TBA to  $\text{H}_2\text{O}_2$  was 20:1, the  $\text{UV}_{254}$  removal rate decreased from 42.2% to 19.4%, i.e., a 22.8% decrease. The main ROS in the  $\text{MoS}_2/\text{Fe}^0/\text{H}_2\text{O}_2$  system was  $\text{HO}^\bullet$ , with  $\text{HO}^\bullet$  being essential for the degradation of refractory organic matter.

Fig.2(b) shows the formation of  $\text{HO}^\bullet$  in the  $\text{H}_2\text{O}_2$  alone,  $\text{H}_2\text{O}_2/\text{MoS}_2$ ,  $\text{Fe}^0/\text{H}_2\text{O}_2$  and  $\text{MoS}_2/\text{Fe}^0/\text{H}_2\text{O}_2$

systems from 0 to 60 min. The results showed that the  $\text{HO}^\bullet$  concentration did not increase significantly with time in the systems with  $\text{H}_2\text{O}_2$  addition ( $\text{H}_2\text{O}_2$  alone,  $\text{H}_2\text{O}_2/\text{MoS}_2$ ,  $\text{Fe}^0/\text{H}_2\text{O}_2$ , and  $\text{MoS}_2/\text{Fe}^0/\text{H}_2\text{O}_2$ ). The  $\text{HO}^\bullet$  concentrations in the  $\text{H}_2\text{O}_2$  alone and  $\text{H}_2\text{O}_2/\text{MoS}_2$  systems at 60 min were 0.26 and 0.30 mmol/L, respectively. The self-decomposition of  $\text{H}_2\text{O}_2$  in these two systems was slow, which further indicated that  $\text{MoS}_2$  hardly activated  $\text{H}_2\text{O}_2$  in the absence of  $\text{Fe}^0$ . The  $\text{HO}^\bullet$  concentration in the  $\text{Fe}^0/\text{H}_2\text{O}_2$  and  $\text{MoS}_2/\text{Fe}^0/\text{H}_2\text{O}_2$  systems increased rapidly with time. At 60 min, the  $\text{HO}^\bullet$  concentration (3.69 mmol/L) in the  $\text{MoS}_2/\text{Fe}^0/\text{H}_2\text{O}_2$  system was 1.31 times that (2.81 mmol/L) of the  $\text{Fe}^0/\text{H}_2\text{O}_2$  system. The  $\text{HO}^\bullet$  was generated more efficiently in the  $\text{Fe}^0/\text{H}_2\text{O}_2$  heterogeneous Fenton system with  $\text{MoS}_2$  added.

To investigate the role of  $\text{H}_2\text{O}_2$  in the  $\text{MoS}_2/\text{Fe}^0/\text{H}_2\text{O}_2$  system, the residual  $\text{H}_2\text{O}_2$  concentration in the different systems was determined by a spectrophotometric determination using potassium titanium oxalate, and the unit effective utilization of  $\text{H}_2\text{O}_2$  in the different systems was calculated. The results are shown in Fig. 2(c) and (d). In the  $\text{MoS}_2/\text{Fe}^0/\text{H}_2\text{O}_2$  system,  $\text{H}_2\text{O}_2$  was significantly decomposed, while the decomposition of  $\text{H}_2\text{O}_2$  in the  $\text{H}_2\text{O}_2$  alone,  $\text{H}_2\text{O}_2/\text{MoS}_2$ , and  $\text{Fe}^0/\text{H}_2\text{O}_2$  systems was limited. The decomposition of  $\text{H}_2\text{O}_2$  in the  $\text{MoS}_2/\text{Fe}^0/\text{H}_2\text{O}_2$  system was the fastest among the different systems investigated. This was consistent with the fastest oxidation and mineralization of refractory organic matter in the MBR effluent occurring in the  $\text{MoS}_2/\text{Fe}^0/\text{H}_2\text{O}_2$  system. In terms of the amount of  $\text{H}_2\text{O}_2$  consumed by TOC per unit mass, the effective utilization rate of  $\text{H}_2\text{O}_2$  was highest in the  $\text{MoS}_2/\text{Fe}^0/\text{H}_2\text{O}_2$  system, and the ratio of  $\text{H}_2\text{O}_2$  to TOC was 8.1, which highlighted the potential degradation of pollutants in the  $\text{MoS}_2/\text{Fe}^0/\text{H}_2\text{O}_2$  system.

### 3.1.5: Comparison of the Fe ion concentration and homogeneous activation in the system

As shown in Fig. 2(e), with the prolongation of reaction time, the  $\text{Fe}^{2+}$  and total Fe concentrations in the two systems increased, with higher concentrations in the  $\text{MoS}_2/\text{Fe}^0/\text{H}_2\text{O}_2$  system than in the  $\text{Fe}^0/\text{H}_2\text{O}_2$  system. The  $\text{Fe}^{3+}$  concentration was calculated by the difference between the total Fe and  $\text{Fe}^{2+}$  concentrations in Fig. 2(e). The  $\text{Fe}^{3+}$  concentration in both the  $\text{Fe}^0/\text{H}_2\text{O}_2$  and  $\text{MoS}_2/\text{Fe}^0/\text{H}_2\text{O}_2$  systems increased gradually with time, while the  $\text{Fe}^{2+}$  concentration increased slowly with time between 0 and 20 min. When the reaction time was prolonged to 30 min, the  $\text{Fe}^{2+}$  concentration decreased from 11.62 and 10.23 mg/L to 10.86 and 7.80 mg/L in the two systems, respectively. The reaction rate of  $\text{HO}^\bullet$  and  $\text{Fe}^{3+}$  generated by the reaction of  $\text{Fe}^{2+}$  and  $\text{H}_2\text{O}_2$  was

too fast, while the rate of  $\text{Fe}^{3+}$  reduced to  $\text{Fe}^{2+}$  was too slow (Eq. (3) and (4)), resulting in a lack of  $\text{Fe}^{3+}$  recovery. However, for the same reaction time, the  $\text{Fe}^{2+}$  concentration in the  $\text{MoS}_2/\text{Fe}^0/\text{H}_2\text{O}_2$  system was always higher than that in the  $\text{Fe}^0/\text{H}_2\text{O}_2$  system. It was confirmed that the presence of  $\text{MoS}_2$  could accelerate the transformation of  $\text{Fe}^{3+}$  to  $\text{Fe}^{2+}$  (Eq. (6)); thus, improving the transformation rate of  $\text{Fe}^{3+}$  to  $\text{Fe}^{2+}$ .

To study the effect of the slow release of  $\text{Fe}^0$  on organic matter removal in the  $\text{MoS}_2/\text{Fe}^0/\text{H}_2\text{O}_2$  system, the  $\text{Fe}^0$  was replaced with different  $\text{Fe}^{2+}$  concentrations (5, 10, and 20 mg/L), as shown in Fig. 2(f). When the  $\text{Fe}^{2+}$  concentration was 5 mg/L, the  $\text{UV}_{254}$  and CN removal rates from the refractory organic matter in the MBR effluent were low. When the dosage of  $\text{Fe}^{2+}$  was increased to 10 mg/L, the  $\text{UV}_{254}$  removal rate increased to 20%. However, a further increase in the  $\text{Fe}^{2+}$  dosage to 10 mg/L did not significantly improve the  $\text{UV}_{254}$  removal rate. In addition, the overall organic matter removal efficiency of the  $\text{Fe}^{2+}/\text{H}_2\text{O}_2/\text{MoS}_2$  system was almost 30% lower than that of the  $\text{MoS}_2/\text{Fe}^0/\text{H}_2\text{O}_2$  system. The  $\text{MoS}_2/\text{Fe}^0/\text{H}_2\text{O}_2$  system was a long-acting oxidation system with high reactivity.

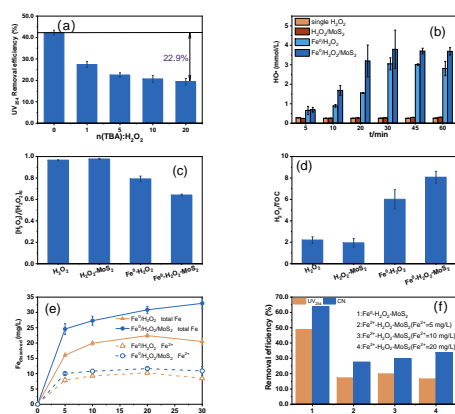


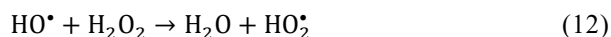
Fig. 2. (a) Effect of a  $\text{HO}^\bullet$  quencher on MBR effluent treated in the  $\text{MoS}_2/\text{Fe}^0/\text{H}_2\text{O}_2$  system. (b) The  $\text{HO}^\bullet$  concentration in different treatment systems. The  $\text{H}_2\text{O}_2$  residual concentration (c) and unit effective efficiency of  $\text{H}_2\text{O}_2$  (d) in different treatment systems. A comparison of the  $\text{Fe}$  ion leaching concentration (e) and organic matter removal efficiency (f)

## 3.2 Factors influencing the degradation of refractory organic matter in MBR effluent by $\text{MoS}_2/\text{Fe}^0/\text{H}_2\text{O}_2$

### 3.2.1: The $\text{H}_2\text{O}_2$ dosage

As shown in Fig. 3(a), when the  $\text{H}_2\text{O}_2$  dosage increased from 1 to 40 mmol/L, the  $\text{UV}_{254}$  and CN

removal efficiency increased significantly from 18.10% and 29.27–46.92% and 61.34%, respectively. However, when the  $\text{H}_2\text{O}_2$  dosage continued to increase to 60 mmol/L, the organic matter removal rate decreased slightly. Increasing the  $\text{H}_2\text{O}_2$  dosage in the  $\text{MoS}_2/\text{Fe}^0/\text{H}_2\text{O}_2$  system increased the yield of  $\text{HO}^\bullet$  to a certain extent; thus, improving the organic matter removal efficiency. However, when the  $\text{H}_2\text{O}_2$  concentration was too high, it operated as a  $\text{HO}^\bullet$  quencher (Eq. (12)).

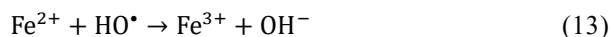


### 3.2.2 The $\text{MoS}_2$ dosage

As shown in Fig. 3(b), the addition of  $\text{MoS}_2$  enhanced the performance of the  $\text{Fe}^0/\text{H}_2\text{O}_2$  system in degrading the refractory organic matter in the leachate. When the  $\text{MoS}_2$  dosage was in the range of 0–0.1 g/L, with the increase in  $\text{MoS}_2$ , the  $\text{UV}_{254}$  and CN removal rates increased from 30.58% and 43.77–48.68% and 63.26%, respectively, and  $k$  increased from 0.012 to  $0.024 \text{ min}^{-1}$ . This was attributed to the action of  $\text{MoS}_2$  and  $\text{Fe}^0$  (Eq. (6) and (7)), which accelerated the rate limiting step of  $\text{Fe}^{3+}$  to  $\text{Fe}^{2+}$  transformation in the heterogeneous Fenton process. The  $\text{UV}_{254}$  and CN removal rates decreased slightly when the  $\text{MoS}_2$  dosage continued to increase (from 0.1 to 0.2 g/L), and therefore, the surplus  $\text{MoS}_2$  had an inhibitory effect on the leachate degradation process. This was probably because some free  $\text{Mo}^{4+}$  eliminated  $\text{HO}^\bullet$  and inhibited degradation.

### 3.2.3: The $\text{Fe}^0$ dosage

As a heterogeneous activator,  $\text{Fe}^0$  played an important role in the degradation of pollutants in the  $\text{MoS}_2/\text{Fe}^0/\text{H}_2\text{O}_2$  system. As shown in Fig. 3(c), when the  $\text{Fe}^0$  dosage increased from 0.05 to 0.4 g/L, the  $\text{UV}_{254}$  and CN removal efficiency in the leachate increased from 15.29% and 36.56–44.29% and 60.43% after 30 min of reaction, and the corresponding reaction rate increased from 0.006 to  $0.020 \text{ min}^{-1}$ . The increase in  $\text{Fe}^0$  dosage increased the release of dissolved  $\text{Fe}^{2+}$ ; thus, promoting the decomposition of  $\text{H}_2\text{O}_2$  to  $\text{HO}^\bullet$ . In contrast, the  $\text{UV}_{254}$  and CN removal efficiencies in leachate at an  $\text{Fe}^0$  dosage greater than 0.4 g/L tended to level off. At a higher  $\text{Fe}^0$  dosage, the degradation of organic matter in the leachate may be due to the  $\text{HO}^\bullet$  consumed by  $\text{Fe}^{2+}$  (Eq. (13)).



### 3.2.4: The initial pH

The initial pH significantly affected the release of  $\text{Fe}^{2+}$  and influenced the interaction of  $\text{MoS}_2$  with  $\text{Fe}^0$ . The effect of different initial pH values (3–11) on the degradation of organic matter in the effluent was studied. As shown in Fig. 3(d), the  $\text{UV}_{254}$  and CN removal rates at an initial pH=3 were 50.09% and 61.58%, respectively. However, when the initial pH was increased to 5–11, the removal rate of  $\text{UV}_{254}$  was less than 20%. Under acidic conditions, the generation of  $\text{Fe}^{2+}$  was promoted due to the corrosion of  $\text{Fe}^0$ , which was beneficial for the generation of  $\text{HO}^\bullet$  to degrade the pollutants. On the other hand, the activity of  $\text{MoS}_2$  was affected in this pH range. Under acidic conditions, the edge S atoms on the  $\text{MoS}_2$  surface may separate and then be captured by  $\text{H}^+$ . However, when the pH value increased, the S atoms cannot be captured; thus, hindering the exposure of  $\text{Mo}^{4+}$ .

### 3.2.5: The reaction time

As shown in Fig. 3(e), when the initial pH=3,  $\text{H}_2\text{O}_2$ =40 mmol/L,  $\text{Fe}^0$ =0.4 g/L, and  $\text{MoS}_2$ =0.1 g/L, with the prolongation of reaction time, the  $\text{UV}_{254}$  and CN removal rates in the MBR effluent increased from 18.54% and 35.32% at 5 min to 55.18% and 65.12% at 60 min, respectively. Correspondingly, with the prolongation of reaction time, due to the limitation of oxidizer and reaction substrate, the organic matter removal rate increased slowly. In addition, the  $\text{UV}_{254}$  removal conformed to pseudo first-order kinetics, and the fitting results are shown in Fig. 3(f). The  $k_{\text{UV}_{254}}$  was  $0.0105 \text{ min}^{-1}$ , indicating that the  $\text{HO}^\bullet$  produced a faster removal rate for macromolecules and aromatic organic matter. Fig. S2 and Table S3 also show that the humus in leachate decreased substantially with the prolongation of reaction time, with humus removal rates in the ultraviolet and visible regions reaching 74.21% and 61.40%, respectively, at 60 min. However, with a reaction time from 30 to 60 min, the  $\text{UV}_{254}$  removal rate increased by less than 10%.

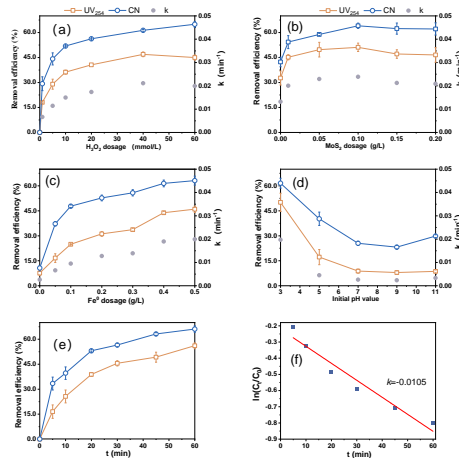


Fig. 3. Effect of different experimental conditions on the organic matter removal rate of the  $\text{Fe}^0/\text{H}_2\text{O}_2$  system enhanced by  $\text{MoS}_2$ : (a)  $\text{H}_2\text{O}_2$  dosage, (b)  $\text{MoS}_2$  dosage, (c)  $\text{Fe}^0$  dosage, (d) different initial pH values, and (e)

## 3.3 Enhancement of the $\text{Fe}^0/\text{H}_2\text{O}_2$ system by $\text{MoS}_2$

### 3.3.1: Analysis of the $\text{Fe}^0$ characteristics before and after the reaction

Scanning electron microscopy and EDS were used to study the surface morphology and elemental composition of  $\text{Fe}^0$  before and after the reaction in the  $\text{Fe}^0/\text{H}_2\text{O}_2$  and  $\text{Fe}^0/\text{H}_2\text{O}_2$  systems enhanced by  $\text{MoS}_2$ . The results are shown in Fig. 4. The  $\text{Fe}^0$  surface before the reaction was uneven (Fig. 4(a)), with a specific pore structure and metallic luster, and the Fe content of the material before the reaction was 100%. Many amorphous crystalline substances were generated on the surface of the Fe material after 30 min of reaction in the two systems, resulting in a rough  $\text{Fe}^0$  surface after the reaction. In addition, it was observed that the surface of the  $\text{Fe}^0$  material in the  $\text{MoS}_2/\text{Fe}^0/\text{H}_2\text{O}_2$  system (Fig. 4(c)) was relatively smoother than that in the  $\text{Fe}^0/\text{H}_2\text{O}_2$  system (Fig. 4(b)), which may have been caused by the generation of more nanoscale metal oxides ( $\text{Fe}_2\text{O}_3$ ,  $\text{CaO}$ ,  $\text{MgO}$ , etc.) on the material surface. The Fe content (53.41%) decreased and the O content (42.53%) increased in the  $\text{MoS}_2/\text{Fe}^0/\text{H}_2\text{O}_2$  system. This indicated that  $\text{Fe}^0$  was susceptible to O absorbing corrosion under acidic conditions, and iron oxides formed on the surface during the oxidation in the  $\text{MoS}_2/\text{Fe}^0/\text{H}_2\text{O}_2$  system.

### 3.2.3: The $\text{Fe}^{3+}/\text{Fe}^{2+}$ redox cycle and $\text{MoS}_2$ conversion mechanism

To study the change in phase composition before and after the reaction of  $\text{Fe}^0$ ,  $\text{Fe}^0$  before and after the reaction in the two systems was characterized by XRD. As shown in Fig. 4(d), the characteristic crystallographic planes of  $\text{Fe}^0$  appeared in the X-ray maps of  $\text{Fe}^0$  before the reaction, i.e., (110), (200), and (211), which corresponded to the diffraction peaks at  $44.6^\circ$ ,  $65.0^\circ$ , and  $82.3^\circ$  in the plots, respectively, in agreement with  $\text{Fe}^0$  (Joint Committee on Powder Diffraction Standards (JCPDS) standard card PDF#06–0696). The diffraction peak at  $2\theta=44.6^\circ$  in the  $\text{MoS}_2/\text{Fe}^0/\text{H}_2\text{O}_2$  system clearly weakened after the reaction, but the overall diffraction peak was consistent with that before the reaction. This may be because only a small amount of iron oxide or iron hydroxide formed on the  $\text{Fe}^0$  surface after the reaction, and it could not be detected by XRD. We then used XPS to analyze the elemental components of the materials after the reactions in the  $\text{Fe}^0/\text{H}_2\text{O}_2$  and  $\text{MoS}_2/\text{Fe}^0/\text{H}_2\text{O}_2$



systems.

From the full XPS spectrum (Fig. S3) it was apparent that there were three strong photoelectron lines of Fe (2p), O (1s), and Mo (3d) in the XPS spectrum. This indicated the presence of the three elements, Fe, O, and Mo, on the surface of the material. To further study the valence changes of Fe, O, and Mo during the reaction, an XPS-peak differentiation analysis was conducted for Fe, O, and Mo, and the specific peak differentiation results are shown in Table S4. Fig. 4(e) is a high-resolution XPS optical map of O1 s. Two peaks were identified at 530.2 and 531.6 eV, corresponding to the Fe-O and Fe-OH bonds in the material, respectively. This indicates that during the reaction process in the  $\text{Fe}^0/\text{H}_2\text{O}_2$  and  $\text{MoS}_2/\text{Fe}^0/\text{H}_2\text{O}_2$  systems some iron (hydrated) oxides (such as  $\text{Fe}_2\text{O}_3$ ,  $\text{Fe}_3\text{O}_4$ , and  $\text{FeOOH}$ ) formed and were present on the surface of  $\text{Fe}^0$  as mixtures, but  $\text{Fe}^0$  was still the main component, which was consistent with the SEM-EDS results.

The fitting results for Fe and Mo are shown in Fig. 4(f) and (g), respectively. The value 719.3 and 733.1 eV in the Fe 2p curves represent the oscillatory satellite energies of Fe 2p<sub>3/2</sub> and Fe 2p<sub>1/2</sub>, respectively. The XPS spectra of  $\text{Fe}^0$  before and after the reaction in  $\text{Fe}^0/\text{H}_2\text{O}_2$  were similar to those in the  $\text{MoS}_2/\text{Fe}^0/\text{H}_2\text{O}_2$  system, with the main difference lying in the different proportions of Fe ions in each system. According to previous studies,  $\text{Fe}^0$  also had two main peaks of Fe2p 3/2 and Fe2p 1/2 after the reaction. The binding energies of 712.4 and 726.0 eV indicated the presence of  $\text{Fe}^{3+}$ , while the binding energies of 710.7 and 724.3 eV were attributed to  $\text{Fe}^{2+}$ . The fitted peak areas according to Fe2p are shown in Table S4. The  $\text{Fe}^{2+}$  and  $\text{Fe}^{3+}$  in the  $\text{Fe}^0/\text{H}_2\text{O}_2$  system accounted for 42.9% and 57.1% of the Fe ions, respectively, and  $\text{Fe}^{2+}$  accounted for 47.5% of the Fe ions in the  $\text{MoS}_2/\text{Fe}^0/\text{H}_2\text{O}_2$  system. This indicated that the presence of  $\text{MoS}_2$  increased the conversion rate of  $\text{Fe}^{3+}$  to  $\text{Fe}^{2+}$ .

From Eq. (6), as  $\text{Fe}^{3+}$  was reduced to  $\text{Fe}^{2+}$ ,  $\text{Mo}^{4+}$  was oxidized to  $\text{Mo}^{6+}$ . According to previous studies, unsaturated S atoms on the surface of  $\text{MoS}_2$  could be removed by capturing protons in the solution. Therefore,  $\text{Mo}^{4+}$  exposed on the surface of  $\text{MoS}_2$  became very active. This was conducive to the transformation of  $\text{Fe}^{3+}$  into  $\text{Fe}^{2+}$ . The XPS results confirmed the oxidation of the exposed  $\text{Mo}^{4+}$ . In Fig. 4(g), the Mo3d peak of  $\text{MoS}_2$  before and after the reaction moved slightly in the direction of the high binding energy. This was attributed to the reduction of the electron cloud of Mo3d. As  $\text{Mo}^{4+}$  was oxidized to  $\text{Mo}^{6+}$ , the electrons of  $\text{Mo}^{4+}$  were captured by  $\text{Fe}^{3+}$  in the reaction solution, which resulted in a decrease in the electron cloud density of  $\text{Mo}^{4+}$ , and

the XPS peak of  $\text{Mo}^{4+}$  moved in the direction of the high binding energy. In addition, the Mo3d XPS spectrum after the  $\text{MoS}_2$  reaction had a new peak at 235.7 eV, corresponding to  $\text{Mo}^{6+}$ , which further proved that  $\text{Mo}^{4+}$  was oxidized to  $\text{Mo}^{6+}$ . The characteristic peak of  $\text{Mo}^{6+}$  was very weak, which may be due to the reduction of  $\text{Mo}^{6+}$  to  $\text{Mo}^{4+}$  in the presence of  $\text{H}_2\text{O}_2$ . These results further confirm that Eq. (6) and (7) can be used for the degradation and even mineralization of refractory organic matter in MBR effluent in the  $\text{MoS}_2/\text{Fe}^0/\text{H}_2\text{O}_2$  system.

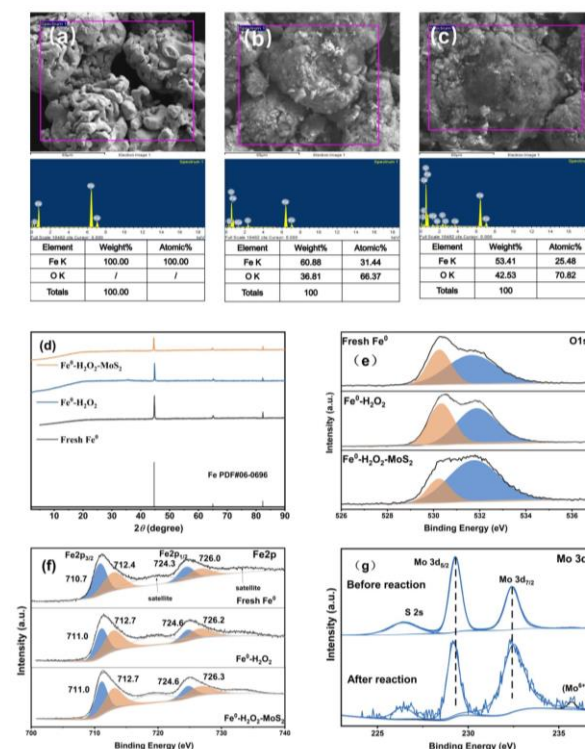


**Fig. 4.** Scanning electron microscope images and energy dispersive spectrometer spectra of  $\text{Fe}^0$  before the reaction in the  $\text{Fe}^0/\text{H}_2\text{O}_2$  system (a),  $\text{MoS}_2/\text{Fe}^0/\text{H}_2\text{O}_2$  system (b), and after the reaction (c). (d) The XRD patterns of  $\text{Fe}^0$  before and after the reaction in the  $\text{Fe}^0/\text{H}_2\text{O}_2$  and  $\text{MoS}_2/\text{Fe}^0/\text{H}_2\text{O}_2$  systems. (e–f) The XPS patterns of O, Fe, and Mo before and after the reaction in the  $\text{Fe}^0/\text{H}_2\text{O}_2$  and  $\text{MoS}_2/\text{Fe}^0/\text{H}_2\text{O}_2$  systems.

### **3.4 The application of the $\text{MoS}_2/\text{Fe}^0/\text{H}_2\text{O}_2$ system to several aromatic model pollutants**

### 3.4.1 : The degradation efficiency of aromatic model pollutants in the MoS<sub>2</sub>/Fe<sup>0</sup>/H<sub>2</sub>O<sub>2</sub> system

Bisphenol A (BPA), IBU, and CIP are typical constituents of the refractory organic matter in leachate. To prove the effectiveness of the MoS<sub>2</sub>/Fe<sup>0</sup>/H<sub>2</sub>O<sub>2</sub> system in the degradation of these aromatic pollutants, their degradation efficiencies in the Fe<sup>0</sup>/H<sub>2</sub>O<sub>2</sub> and MoS<sub>2</sub>/Fe<sup>0</sup>/H<sub>2</sub>O<sub>2</sub> systems were compared. Considering that the composition of the model pollutants was not as complex as that of leachate, the dosage of oxidant and activator in the system was adjusted correspondingly. The results are shown in Fig. 5(a).

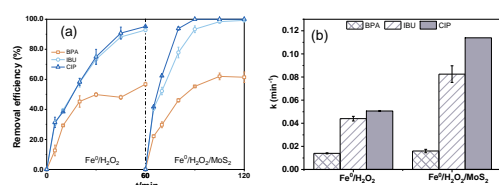


Fig. 5. Removal efficiency (a) and reaction rate (b) of IBU, BPA, and CIP in the Fe<sup>0</sup>/H<sub>2</sub>O<sub>2</sub> and MoS<sub>2</sub>/Fe<sup>0</sup>/H<sub>2</sub>O<sub>2</sub> systems (reaction conditions: initial pH = 3, [BPA] = [IBU] = [CIP] = 40 mg/L, H<sub>2</sub>O<sub>2</sub> = 5 mmol/L, Fe<sup>0</sup> = 0.2 g/L, MoS<sub>2</sub> = 0.02 g/L).

The IBU and CIP removal rates in the MoS<sub>2</sub>/Fe<sup>0</sup>/H<sub>2</sub>O<sub>2</sub> system were in excess of 99% after 30 min, while IBU and CIP were completely removed after 60 min, with degradation rate constants (Fig. 5(b)) of 0.082 and 0.113 min<sup>-1</sup>, respectively. The degradation rate of BPA was only 62%. The biphenyl structure of BPA requires the continuous oxidation of HO<sup>•</sup> to break bonds and open rings. The removal of IBU and CIP in the MoS<sub>2</sub>/Fe<sup>0</sup>/H<sub>2</sub>O<sub>2</sub> system was 1.1 times that in the Fe<sup>0</sup>/H<sub>2</sub>O<sub>2</sub> system, and CIP could be completely eliminated in the MoS<sub>2</sub>/Fe<sup>0</sup>/H<sub>2</sub>O<sub>2</sub> system within 30 min. In addition, the removal rate constant of IBU in the MoS<sub>2</sub>/Fe<sup>0</sup>/H<sub>2</sub>O<sub>2</sub> system (0.082 min<sup>-1</sup>) was 1.9 times higher than that in Fe<sup>0</sup>/H<sub>2</sub>O<sub>2</sub> (0.044 min<sup>-1</sup>). The removal of CIP in the MoS<sub>2</sub>/Fe<sup>0</sup>/H<sub>2</sub>O<sub>2</sub> system (1.13 min<sup>-1</sup>) was 2.2 times higher than in the Fe<sup>0</sup>/H<sub>2</sub>O<sub>2</sub> system (0.051 min<sup>-1</sup>). This indicates that the MoS<sub>2</sub>/Fe<sup>0</sup>/H<sub>2</sub>O<sub>2</sub> system was faster than the Fe<sup>0</sup>/H<sub>2</sub>O<sub>2</sub> system for the removal of the two aromatic model pollutants.

### 3.4.2.: The degradation pathways of IBU, BPA, and CIP

The degradation of aromatic organic matter is usually accompanied by the formation of intermediate

byproducts. These intermediates have strong toxic effects and may present a risk to the environment. Several intermediates produced by IBU, BPA, and CIP in the MoS<sub>2</sub>/Fe<sup>0</sup>/H<sub>2</sub>O<sub>2</sub> system were identified by LC-TOF-MS. The possible degradation pathways of IBU, BPA, and CIP in the MoS<sub>2</sub>/Fe<sup>0</sup>/H<sub>2</sub>O<sub>2</sub> system were proposed as follows.

(1) The degradation pathways of the nonsteroidal anti-inflammatory drug IBU.

Based on the data from this and related studies, three possible degradation pathways of IBU were speculated, as shown in Fig. 6(a). Pathway I: Due to the large special steric hindrance of the 2-methylpropyl group on the side chain of IBU, HO<sup>•</sup> preferentially attacks the para-position to form the corresponding hydroxylation product (P2 *m/z* 220) and forms 1-[4-(2-methylpropyl) phenyl] ethenone (P3 *m/z* 176) under the continuous attack of HO<sup>•</sup>. Pathway II: HO<sup>•</sup> attacks the lipid chain alkyl group of IBU to form an intermediate product (P4 *m/z* 220), and the acyl group is then oxidized to the carboxyl group to form 2-(4-methylphenyl) propanoic acid (P5 *m/z* 164). Pathway III: HO<sup>•</sup> simultaneously attacks the two groups in the para position on the benzene ring of IBU and forms the corresponding hydroxylated intermediate (P6 *m/z* 237). After oxidation-dehydration, the small organic acid 4-acetyl benzoic acid (P7 *m/z* 164) is formed. Finally, with the continuous attack of HO<sup>•</sup>, some intermediates of these aromatic molecules can form short chain small molecules through ring-opening reactions, such as 5-methylhexan-2-one (P8 *m/z* 114) and (P9 *m/z* 171).

(2) The degradation pathway of the endocrine disruptor BPA.

Fig. 6(b) shows the possible degradation pathway of BPA. First, the electrophilic group (HO<sup>•</sup>) will preferentially attack the densest part of the electron cloud of BPA. Therefore, C2 and C5 are more vulnerable to HO<sup>•</sup>. Then, P2 is produced after hydroxylation, and is converted to carbonyl to form P3 by HO<sup>•</sup> continuous oxidation and further cleavage to small organic acids 2-(3,4-Dioxyidenecyclohex-1,5-dienyl) acetic acid (P4 *m/z* 164). The C-C bond connection between isopropyl and the benzene ring is cleaved by a HO<sup>•</sup> attack, which can be coupled with phenol in solution to form 4-(4-Hydroxyphenyl) benzene-1,2-dione (P5 *m/z* 200). Under the continuous attack of HO<sup>•</sup>, these aromatic compounds gradually split into straight chain compounds, such as hexa-1,5- diene-3,4-diol (P7 *m/z* 114) and methyl 3-hydroxyheptanoate (P8 *m/z* 160).



### (3) The degradation pathway of the antibiotic CIP.

As shown in previous studies, the degradation of quinolones may occur on the piperazine ring and quinolone ring structures. Combined with information from previous studies and the intermediates detected by LC-TOF-MS, a possible pathway of oxidation of CIP in the  $\text{MoS}_2/\text{Fe}^0/\text{H}_2\text{O}_2$  system was proposed, as shown in Fig. 6(c). Because of the high electron affinity of  $\text{OH}^\bullet$ , it will readily attack the piperazine and quinolone rings on CIP. With the opening of the piperazine and quinolone rings of CIP, a series of oxidation and decarboxylation reactions take place, and the small organic molecule 4-fluoroaniline (P8  $m/z$  112) is formed. The piperazine and quinolone structures of CIP molecules could be completely destroyed in the  $\text{MoS}_2/\text{Fe}^0/\text{H}_2\text{O}_2$  system.

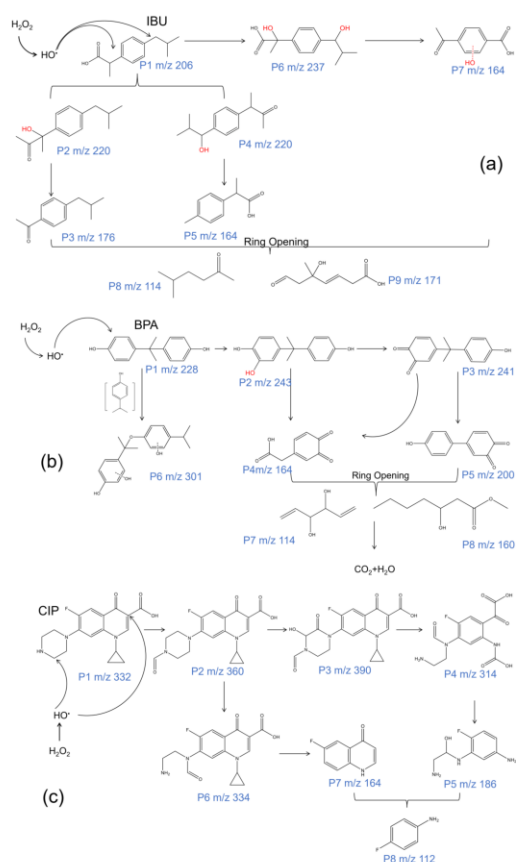


Fig. 6. Degradation pathways of IBU, BPA, and CIP in the  $\text{MoS}_2/\text{Fe}^0/\text{H}_2\text{O}_2$  system (a)–(c).

### 3.4.3: Degradation mechanism

Based on the above results, a possible mechanism for the degradation of refractory organic matter in MBR

effluent in the  $\text{MoS}_2/\text{Fe}^0/\text{H}_2\text{O}_2$  system was proposed. As shown in Fig. 7,  $\text{H}_2\text{O}_2$  was decomposed by the  $\text{Fe}^{2+}$  released from  $\text{Fe}^0$  to generate  $\text{OH}^\bullet$  and  $\text{Fe}^{3+}$  in the solution at the same time. In the  $\text{MoS}_2/\text{Fe}^0/\text{H}_2\text{O}_2$  system, the presence of  $\text{MoS}_2$  helped to convert  $\text{Fe}^{3+}$  into  $\text{Fe}^{2+}$ . First,  $\text{MoS}_2$  captured protons, generating  $\text{H}_2\text{S}$  in solution and forming unsaturated S atoms on the surface of  $\text{MoS}_2$ . Then, the  $\text{Mo}^{4+}$  exposed on the  $\text{MoS}_2$  surface promoted the transformation of  $\text{Fe}^{3+}$  to  $\text{Fe}^{2+}$  through a redox reaction and generated  $\text{Mo}^{6+}$ . Finally, under the action of  $\text{H}_2\text{O}_2$  in solution,  $\text{Mo}^{6+}$  was reduced to  $\text{Mo}^{4+}$  to realize its own cycle. The circulation of Fe ions led to an increase in the  $\text{Fe}^{2+}$  concentration in the solution and further increased the  $\text{HO}^\bullet$  concentration in the system. Finally, due to the characteristics of  $\text{HO}^\bullet$  nonselective oxidation, a series of additions, substitutions, bond breaking, ring opening, and other reactions could occur with pollutants, with the result that macromolecular organic matter with a stable structure or that is difficult to biodegrade was transformed into small molecules that were easy to degrade or even mineralize. In addition, the iron oxides generated on the surface of  $\text{Fe}^0$  had certain adsorption and precipitation effects. To reduce the Fe ion concentration following treatment by the oxidation method in the wastewater, the pH of the effluent in the  $\text{MoS}_2/\text{Fe}^0/\text{H}_2\text{O}_2$  system was adjusted to 9. Because a large number of Fe ions were converted into Fe-based colloids or other flocculants under alkaline conditions, the leached Fe ion concentration was effectively controlled after precipitation and flocculation, and the pollutants were removed by flocculation to a certain extent. In summary, the mechanism of the refractory degradation of organic pollutants in MBR effluent in the  $\text{MoS}_2/\text{Fe}^0/\text{H}_2\text{O}_2$  system could be attributed to the homogeneous and heterogeneous Fenton reaction and the adsorption and precipitation of organic matter by Fe-based colloids.

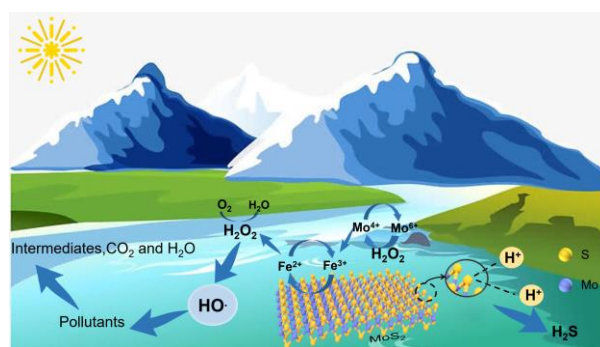


Fig. 7. Mechanism of refractory organic pollutant removal in the effluent produced during the treatment of landfill leachate by an MBR in the  $\text{MoS}_2/\text{Fe}^0/\text{H}_2\text{O}_2$  system.

## 4 CONCLUSIONS

This study analyzed the ability of the  $\text{MoS}_2/\text{Fe}^0/\text{H}_2\text{O}_2$  system to oxidize refractory organic matter in the effluent produced during the treatment of landfill leachate by an MBR, and assessed the synergistic effect of  $\text{MoS}_2$  on the mineralization of organic matter and degradation of humic-like organic matter in different systems. The mechanism of the  $\text{MoS}_2/\text{Fe}^0/\text{H}_2\text{O}_2$  system was proposed through the identification of ROS and a system comparison of the  $\text{HO}^\bullet$  concentration, the effective utilization rate of  $\text{H}_2\text{O}_2$ , the morphology of the materials, and the results of an XRD and XPS analysis. The degradation rate of aromatic organics (e.g., nonsteroidal and quinolones) in the  $\text{MoS}_2/\text{Fe}^0/\text{H}_2\text{O}_2$  system was approximately twice that in the  $\text{Fe}^0/\text{H}_2\text{O}_2$  system. Because  $\text{MoS}_2$  accelerated the  $\text{Fe}^{3+}/\text{Fe}^{2+}$  redox cycle, the system had a higher reactivity and oxidation performance. It was concluded that the  $\text{MoS}_2/\text{Fe}^0/\text{H}_2\text{O}_2$  system was an effective method for the removal of refractory organic matter from MBR effluent following the treatment of landfill leachate.

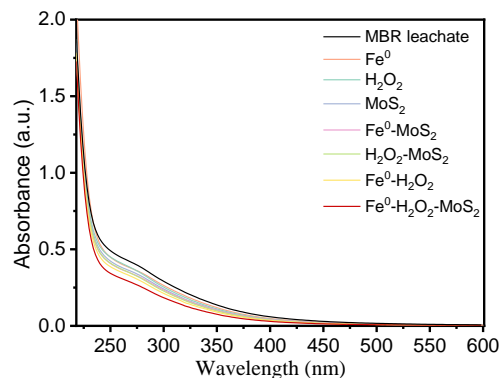


Figure S1. The UV-Vis spectra of MBR effluent treated by different processes.

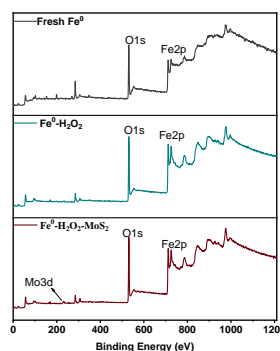


Figure S3. A full-range scan of the XPS spectra of  $\text{Fe}^0$  in the  $\text{Fe}^0/\text{H}_2\text{O}_2$  and  $\text{MoS}_2/\text{Fe}^0/\text{H}_2\text{O}_2$  processes before and after the reaction.

Table S1. Specific absorbance value of MBR effluent treated by different processes.

Type	$A_{254}$	$A_{280}$	$A_{300}/A_{400}$	$A_{240}/A_{420}$	$A_{250}/A_{365}$	$A_{226-400}$
MBR leachate	0.4807	0.3853	4.9144	13.2302	4.6991	52.1834
$\text{Fe}^0$	0.4285	0.3430	5.5378	15.5362	5.1187	46.3047
$\text{H}_2\text{O}_2$	0.4407	0.3469	5.7444	16.7209	5.4495	46.4678
$\text{MoS}_2$	0.4135	0.3283	6.1207	17.8904	5.5909	44.0284
$\text{Fe}^0\text{-MoS}_2$	0.3984	0.3169	5.7422	16.3654	5.3706	42.6049

H <sub>2</sub> O <sub>2</sub> -MoS <sub>2</sub>	0.4007	0.3131	6.0000	18.1762	5.6970	42.1956
Fe <sup>0</sup> -H <sub>2</sub> O <sub>2</sub>	0.3780	0.2945	6.0722	18.3783	5.8446	39.7701
Fe <sup>0</sup> -H <sub>2</sub> O <sub>2</sub> -MoS <sub>2</sub>	0.3353	0.2575	6.3377	20.1915	6.1901	35.2513

Table S2. Variations of peak intensity and peak position of Peak A and Peak C of MBR effluent before and after treatment by different processes.

Type	Peak A	(a u)	efficiency	Peak C	(a u)	efficiency	Peak A/ Peak C
MBR	250.0/460.0	3625.0	/	325.0/410.0	2578.0	/	1.41
H <sub>2</sub> O <sub>2</sub>	250.0/455.0	3857.0	0	325.0/410.0	2844.0	0	1.36
Fe <sup>0</sup>	250.0/450.0	3712.0	0	330.0/415.0	2707.0	0	1.37
MoS <sub>2</sub>	250.0/460.0	3450.0	4.8%	315.0/435.0	2341.0	9.2%	1.47
Fe <sup>0</sup> /MoS <sub>2</sub>	250.0/455.0	3627.0	0	325.0/405.0	2630.0	0	1.38
H <sub>2</sub> O <sub>2</sub> /MoS <sub>2</sub>	250.0/455.0	3396.0	6.3%	325.0/415.0	2488.0	3.5%	1.36
Fe <sup>0</sup> /H <sub>2</sub> O <sub>2</sub>	245.0/410.0	1311.0	63.8%	320.0/405.0	1502.0	41.7%	0.87
Fe <sup>0</sup> /H <sub>2</sub> O <sub>2</sub> /MoS <sub>2</sub>	250.0/420.0	1001.0	72.4%	315.0/410.0	1091.0	57.7%	0.91

Table S4. Peak differentiation results of Fe 2p, O 1s, and Mo 3d.

BE/eV	Peak area	Ratio %
-------	-----------	---------

	Fresh	Fe <sup>0</sup> /H <sub>2</sub> O <sub>2</sub>	Fe <sup>0</sup> /H <sub>2</sub> O <sub>2</sub> /MoS <sub>2</sub>	Fresh	Fe <sup>0</sup> /H <sub>2</sub> O <sub>2</sub>	Fe <sup>0</sup> /H <sub>2</sub> O <sub>2</sub> /MoS <sub>2</sub>	Fresh	Fe <sup>0</sup> /H <sub>2</sub> O <sub>2</sub>	Fe <sup>0</sup> /H <sub>2</sub> O <sub>2</sub> /MoS <sub>2</sub>
O1s	530.2	530.3	530.2	6554	17103	4895	34.4	45.7	23.5
	531.6	531.8	531.7	12479	20287	15957	65.6	54.3	76.5
	712.4	712.7	712.7	6362	21364	11046			
Fe <sup>3+</sup>							45.5	57.1	52.4
	726.0	726.2	726.3	3181	10682	5523			
Fe2p									
	724.3	724.6	724.6	3799	9672	4078			
Fe <sup>2+</sup>							54.42	42.9	47.5
	710.7	711.0	711.0	7598	19345	8157			
	232.4	\	232.4	66815	\	1031	34.1	\	57.6
	229.2	\	229.1	90777	\	478	46.3	\	26.7
Mo3d									
	226.5	\	226.3	38221	\	226	19.5	\	12.6
	\	\	235.7	\	\	54	\	\	0.3